Propeller blade stress estimates using lifting line theory

Brenden Epps[1], Jerod Ketcham[2], and Chryssostomos Chryssostomidis[3]
1: Postdoctoral research associate, MIT Sea Grant College Program
2: Graduate student, MIT Mechanical Engineering
3: Director, MIT Sea Grant College Program and Professor, MIT Mechanical Engineering

Keywords: OPENPROP, propeller design, propeller analysis

Abstract

OPENPROP, an open-source computational tool for the design and analysis of propellers and horizontal-axis turbines, is extended to provide estimates of normal stresses in the blades for both on- and off-design operating conditions. The numerical model is based on propeller lifting theory, and the present implementation of the code includes an analysis capability to estimate the off-design performance of the propeller or turbine and to make blade stress predictions.

As an example, we present the design and performance of a two-bladed propeller. Experimental measurements of the propeller performance over a wide range of off-design operating conditions agree with performance predictions. Estimates of the blade stress are given for on-design and off-design operating states of the propeller.

1. INTRODUCTION

OPENPROP is a suite of open-source propeller and turbine design codes written in the MATLAB programming language [Kimball and Epps 2010]. The codes are based on the same propeller design theory utilized in codes employed by the US Navy for parametric design of marine propellers [Kerwin 2007]. OPENPROP is designed to be a GUI-based user-friendly tool that can be used by both propeller design professionals as well as novices to propeller design.

A team of researchers at MIT, Maine Maritime Academy and University of Maine have contributed to the current OPENPROP code. OPENPROP began in 2001 with the propeller code PVL developed by Kerwin [2007] as part of his MIT propeller design course notes. The first MATLAB version of this code, MPVL, incorporated graphical user interfaces for parametric design and preliminary bladerow design [Chung 2007]. Geometry routines were later added which interfaced with the CAD program Rhino to generate a 3D printable propeller [D'Epagnier et. al. 2007]. These early codes were capable of designing propellers using a simple Lerb's criteria optimizer routine [Lerbs 1952]. Epps et. al. [2009a] implemented a generalized optimizer routine based on the work of Coney [1989] , and Epps [2010] developed an off-design performance analysis capability.

OPENPROP utilizes a lifting-line representation of the blades with constant-diameter helical vortices to represent the blade wake. The computational model incorporates a standard wake alignment procedure to accurately represent moderate blade loading. As such, it can design both propellers and axial flow turbines using the same numerical representation [Epps et. al. 2009].

This paper presents an extension of the code to predict the normal stresses in the blades due to inviscid and viscous loading. The stress analysis currently implemented is applicable to propellers or turbines with zero rake or skew, and extension to the raked or skewed cases is planned. This paper also presents an example propeller design using the current code suite. Experimental measurements of the off-design performance of the propeller are presented for a range of off-design operating conditions. This experimental data provides important validation for the off-design performance analysis capability of OPENPROP. The blade stress estimates for on- and off-design conditions are also shown.

2. METHODOLOGY

What follows is a review of the theoretical foundation and numerical implementation of the OPENPROP code suite, which draws heavily from the theory presented in [Kerwin 2007, Coney 1989, Carlton 1994]. The present implementation of OPENPROP is based on *moderately-loaded lifting line theory*, in which a propeller blade is represented by a lifting line, with trailing vorticity aligned to the local flow velocity (i.e. the vector sum of free-stream plus induced velocity). The induced velocities are computed using a vortex lattice, with helical vortex filaments trailing into the wake at discrete stations along the blade. The blade itself is modeled as discrete sections, having 2D section properties at each radius. Loads are computed by integrating the 2D section loads over the span of the blade. The propeller design optimization procedure determines the optimum circulation distribution along the span of the blade, which yields the minimum torque for a specified thrust, inflow conditions, and blade 2D section properties. For a selected design, the blade shape and pitch angle are determined by scaling 2D section geometry to give the desired on-design loading. The off-design performance is estimated assuming that the lift coefficient of each blade section (and hence, the circulation) is proportional to the local 2D angle of attack, which is computed using the local induced velocity consistent with the blade loading at the off-design condition.

2.1. Propeller lifting line representation

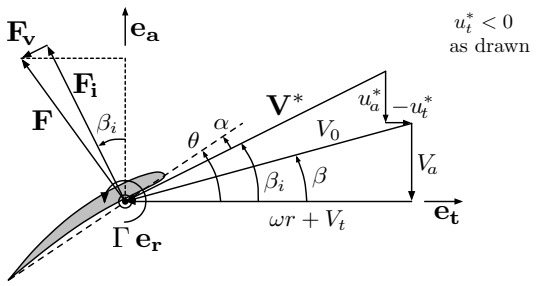

Figure 1. Propeller velocity/force diagram, as viewed from the tip towards the root of the blade. All velocities are relative to a stationary blade section at radius r.

The velocity/force diagram shown in figure 1 illustrates the velocities and forces (per unit span) on a 2D blade section in the axial $\mathbf{e}_a$ and tangential $\mathbf{e}_t$ directions for a propeller rotating with angular velocity $\omega\mathbf{e}_a$. The total resultant inflow velocity, $\mathbf{V}^*$, has magnitude $V^* = \sqrt{(V_a+u_a^*)^2+(\omega r+V_t+u_t^*)^2}$ and is oriented at pitch angle,

$$\beta_i = \tan^{-1}\left[\frac{V_a+u_a^*}{\omega r+V_t+u_t^*}\right] \tag{1}$$

to the $\mathbf{e}_t$ axis. Also shown on figure 1 are the angle of attack, α; blade pitch angle $\theta = \alpha+\beta_i$; circulation, $\Gamma\mathbf{e}_r$; (inviscid) Kutta-Joukowski lift force $F_i = \rho V^*\Gamma$ normal to $\mathbf{V}^*$; and viscous drag force, $F_v = \frac{1}{2}\rho(V^*)^2 C_D c$ aligned with $\mathbf{V}^*$, where ρ is the fluid density, C_D is the drag coefficient, c is the section chord. These forces can be projected into axial and tangential components

$$\mathbf{F_a} = [F_i\cos\beta_i - F_v\sin\beta_i]\ (\mathbf{e}_a) \tag{2}$$
$$\mathbf{F_t} = [F_i\sin\beta_i + F_v\cos\beta_i]\ (-\mathbf{e}_t) \tag{3}$$

Assuming the Z blades are identical, the total thrust and torque on the propeller are

$$\mathbf{T} = Z\int_{r_h}^{R}\mathbf{F_a}\,dr \tag{4}$$
$$\mathbf{Q} = Z\int_{r_h}^{R}(r\,\mathbf{e_r})\times\mathbf{F_t}\,dr \tag{5}$$

where r_h and R are the radius of the propeller hub and tip, respectively.

The axial and tangential induced velocities, $\{u_a^*, u_t^*\}$ are computed using the standard propeller lifting line model, in which the Z propeller blades are each modeled as a set of M horseshoe vortex elements (which consist of a segment of the lifting line and two helical trailing vortices that extend to infinity). Since circulation is assumed constant on each panel, the influence of the vortex lattice at a given radial location, $r_c(m)$, $m = 1\ldots M$, is given by

$$u_a^*(r_c(m)) = \sum_{i=1}^{M}\Gamma(i)\bar{u}_a^*(m,i) \tag{6}$$
$$u_t^*(r_c(m)) = \sum_{i=1}^{M}\Gamma(i)\bar{u}_t^*(m,i) \tag{7}$$

where $\bar{u}_a^*(m,i)$ and $\bar{u}_t^*(m,i)$ are the axial and tangential velocity induced at $r_c(m)$ by a unit-strength horseshoe vortex surrounding the i^{th} panel of each of the Z blades. These influence matrices are functions of $\{Z, r_c(m), r_v(i), \beta_i(i)\}$, which are computed using the approximations by Wrench [1957].

2.2. Off-design performance analysis

An off-design (*OD*) operating state is defined by an off-design advance coefficient,

$$J_{OD} = \frac{V_s}{n_{OD}D} = \frac{\pi V_s}{\omega_{OD}R} \quad , \tag{8}$$

and state variables $\{V^*, \alpha, C_L, \Gamma, u_a^*, u_t^*, \beta_i, \bar{u}_a^*, \bar{u}_t^*\}$. The off-design state is found using a modified Newton solver approach. During each iteration, one Newton solver iteration is performed to drive the residual vector

$$\mathbf{R} = \begin{bmatrix} V^* - \sqrt{(V_a+u_a^*)^2+(\omega_{OD}r_c+V_t+u_t^*)^2} \\ \alpha - (\theta-\beta_i) \\ C_L - (2\pi(\alpha-\alpha_I)+C_{L_I}) \\ \Gamma - \left(\frac{1}{2}C_L V^* c\right) \\ u_a^* - [\bar{u}_a^*]\cdot[\Gamma] \\ u_t^* - [\bar{u}_t^*]\cdot[\Gamma] \end{bmatrix} \tag{9}$$

towards zero. Note that the third residual is merely notional, and a more accurate $C_L(\alpha)$ curve is currently employed in OPENPROP to treat section stall properties [Epps 2010]. Given the new values of $\{V^*, \alpha, C_L, \Gamma, u_a^*, u_t^*\}$, the parameters $\{\beta_i, \bar{u}_a^*, \bar{u}_t^*\}$ are then updated. These new values are used in the next Newton iteration, and so on. This process repeats until convergence of the entire system. For each operating state, the analyzer computes the propeller thrust, torque, and power coefficients and the efficiency [Epps et. al. 2009].

2.3. Blade stress estimation

Given the design state or an off-design state, the blade stresses may be estimated by an application of beam bending theory [Kerwin and Hadler 2010]. The basic assumptions herein are: (1) the blade acts as a cantilevered beam, (2) normal stresses are due to bending and centrifugal forces, (3) sheer stresses are negligible, and (4) the blade has zero rake and skew.

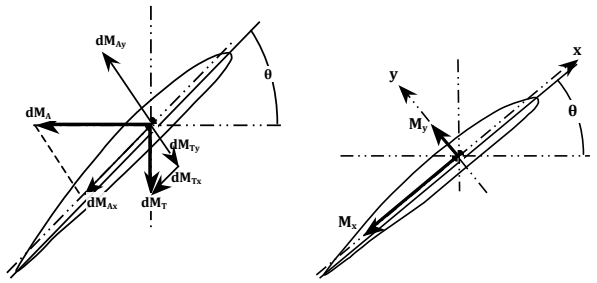

Figure 2. Bending moments and resultants.

Parameter	Value	Description
Z	2	number of blades
N	480 [RPM]	rotation rate ($n = 8$ rev/s)
D	0.25 [m]	diameter (≈ 10 in)
T	30 [N]	required thrust
Vs	1.5 [m/s]	free-stream speed
D_{hub}	0.08382 [m]	hub diameter (3.3 in)
M	20	number of vortex panels

Table 1. Propeller design input parameters.

Centrifugal forces contribute to the overall tensile stress at each blade section. The elemental centrifugal force acting on a blade section from an adjoining section is $dF_c = \omega^2 r\, dm$, where $dm = \rho_b A\, dr$ is the mass of the adjoining section, ρ_b is the propeller blade material density, and A is the section area. The total centrifugal force at a section of radius, r_o, is the sum of the contributions of all outboard sections

$$\mathbf{F_c} = \rho_b \omega^2 \int_{r_o}^{R} A r\, dr \quad (\mathbf{e_r}) \tag{10}$$

which produces tensile stress F_c/A.

Axial and tangential loads contribute to bending stresses at each blade section. The bending stresses at radius r_o are computed from the bending moments about the negative axial and tangentail axes, which are as follows:

$$\mathbf{M_a} = \int_{r_o}^{R} (r - r_o) F_a\, dr \quad (-\mathbf{e_t}) \tag{11}$$

$$\mathbf{M_t} = \int_{r_o}^{R} (r - r_o) F_t\, dr \quad (-\mathbf{e_a}) \tag{12}$$

Since the blade is oriented at pitch angle θ to the $\mathbf{e_t}$ axis, the axial and tangential bending moments are projected onto the centroidal axes (x parallel to the chord line, and y toward the suction side), as shown in figure 2

$$\mathbf{M_x} = M_a \cos\theta + M_t \sin\theta \quad (-\mathbf{e_x}) \tag{13}$$

$$\mathbf{M_y} = M_a \sin\theta - M_t \cos\theta \quad (\mathbf{e_y}) \tag{14}$$

Thus, the total normal stress at point (x, y) of the section is:

$$\sigma(x,y) = -\frac{M_x y}{I_x} - \frac{M_y x}{I_y} + \frac{F_c}{A} \tag{15}$$

where x and y are measured from the centroid of the area of the section. Equation (15) assumes that the blade does not have rake or skew, which would introduce additional bending moments due to F_c.

This procedure is implemented in OPENPROP to estimate the stress for the on-design loading or any off-design state. Since the blade stress requires the loading in physical units, the actual value of V_s or n must be specified, in addition to the non-dimensional off-design advance coefficient. Further details of this procedure are given in [Ketcham 2010].

3. EXAMPLE: PROPELLER DESIGN AND STRESS ANALYSIS

A two-bladed propeller was designed for use in this study. The propeller was designed to operate in the test set-up that will be described shortly. Performance measurements were made at the MIT recirculating water tunnel over a range of off-design operating states. The blade stress was estimated for both on- and off-design conditions, although measurements of the stress were not made.

The primary design parameters are listed in table 1, and their justification follows. The inflow velocity profile was not measured prior to propeller design and assumed uniform ($V_a/V_s = 1$ for all blade sections). The swirl inflow velocity was zero ($V_t = 0$), and the propeller had zero rake or skew. The section drag coefficient was assumed to be $C_D = 0.010$ for all blade sections.

The hub diameter ($D_{\text{hub}} = 3.3$ in) was chosen to match the diameter of the trolling motor used in the experiments. The propeller diameter ($D = 0.25$ m ≈ 10 in) was chosen to be as large as possible while still leaving sufficient clearance to the walls of the water tunnel to mitigate blockage effects. The choice of two blades ($Z = 2$) was driven by the size of the Dimension Elite 3D printer used to fabricate the propeller, which has an 8-inch by 12-inch planform area for printing. Thus, a two-bladed propeller could be printed with a 10-inch diameter, whereas a propeller with three or more blades would be restricted to maximum a diameter of 8 inches. The free-stream speed and thrust were chosen to give a thrust coefficient typical of a marine propeller (see table 2) while having low enough torque that the trolling motor could drive the propeller.

The propeller circulation distribution was optimized in OPENPROP using the [Coney 1989] method, and the non-dimensional design performance of this optimized propeller is shown in table 2. The values for KT and J_s meet those prescribed by the input parameters, and the torque coefficient and efficiency are typical for this loading. Tabulated flow parameters for blade sections at the control points are given in table 3.

The blade shape was chosen to give a reasonably large chords for most of the span, while also maintaining a rounded

$J_s = \frac{V_s}{nD}$	0.75	advance ratio
$KT = \frac{T}{\rho n^2 D^4}$	0.1200	thrust coefficient
$KQ = \frac{Q}{\rho n^2 D^5}$	0.0204	torque coefficient
$EFFY = \frac{TV_s}{Q\omega}$	0.7019	efficiency

Table 2. Design performance parameters.

r/R	G	$\frac{c}{D}$	$\frac{f_0}{c}$	$\frac{t_0}{c}$	θ
0.3517	0.0464	0.2411	0.0453	0.1449	41.6029
0.3845	0.0467	0.2494	0.0414	0.1351	38.9058
0.4173	0.0473	0.2571	0.0383	0.1261	36.5226
0.4502	0.0479	0.2646	0.0356	0.1179	34.4033
0.4830	0.0484	0.2713	0.0332	0.1103	32.5101
0.5158	0.0487	0.2769	0.0310	0.1035	30.8108
0.5486	0.0489	0.2822	0.0291	0.0972	29.2759
0.5815	0.0489	0.2864	0.0272	0.0914	27.8841
0.6143	0.0486	0.2886	0.0256	0.0862	26.6175
0.6471	0.0481	0.2901	0.0241	0.0813	25.4575
0.6799	0.0473	0.2911	0.0226	0.0768	24.3908
0.7128	0.0463	0.2911	0.0212	0.0726	23.4068
0.7456	0.0449	0.2889	0.0199	0.0686	22.4980
0.7784	0.0431	0.2849	0.0186	0.0650	21.6553
0.8113	0.0409	0.2795	0.0173	0.0619	20.8710
0.8441	0.0381	0.2692	0.0162	0.0592	20.1432
0.8769	0.0348	0.2539	0.0151	0.0567	19.4651
0.9097	0.0305	0.2348	0.0138	0.0543	18.8277
0.9426	0.0250	0.2052	0.0125	0.0519	18.2297
0.9754	0.0171	0.1470	0.0115	0.0541	17.6748

Table 3. Optimized blade design: radius/propeller radius, r/R; non-dimensional circulation, $G = \frac{\Gamma}{2\pi R V_s}$; chord/diameter, $\frac{c}{D}$; camber ratio, $\frac{f_0}{c}$; and thickness ratio, $\frac{t_0}{c}$; and blade pitch angle, θ [deg]. The chord lengths were not optimized.

blade tip. Large chord lengths enable large blade thickness (required so the blade would not flex during testing) while still having small thickness to chord ratio (required for linear foil theory). The 2D foil section thickness profile was a version of the *'NACA 65A010'* thickness form]Abbott and von Doenhoff, 1959, p. 369], which was modified slightly to be amenable to 3D printing. The *'NACA 65A010'* and *'NACA 65A010 (modified)'* forms are shown in figure 3. The modified shape was obtained by truncating and rounding the trailing edge and then stretching the aft half of the blade section to be the original length. Further details of the design are given in [Epps 2010].

The 3D blade geometry was built from 2D sections, as described in [Epps 2009a]. The geometry of each 2D section is defined by the meanline camber profile and thickness forms. The meanline selected was the *'NACA a=0.8*

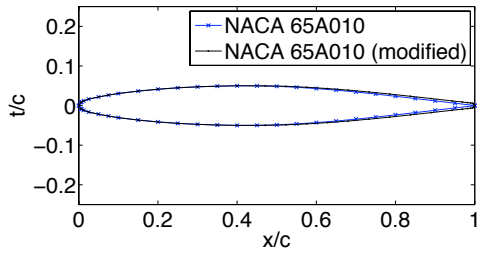

(b)

Figure 3. Blade thickness form: 'NACA65A010' versus 'NACA65A010 (modified)'.

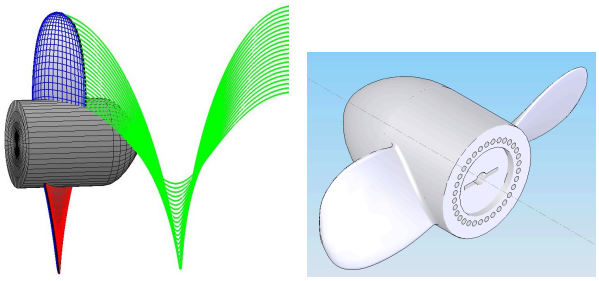

Figure 4. Rendering of the propeller blades: (a) OPENPROP, (b) SolidWorks.

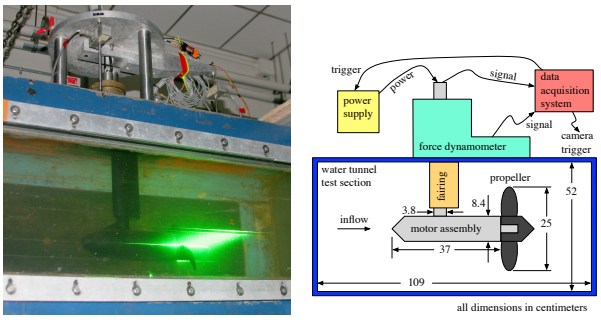

Figure 5. Propeller test setup: power is delivered to and Hall-effect signal is acquired from the motor assembly by umbilical. The data acquisition system triggers the power supply and PIV camera to start the unsteady start-up tests.

(modified)' meanline type [Abbott and von Doenhoff, 1959, p. 403]. This meanline type has an ideal lift coefficient of $\widetilde{C_{L_I}} = 1.0$ and an ideal angle of attack of $\widetilde{\alpha}_I = 1.40$ with a maximum camber ratio of $\tilde{f}_0/c = 0.06651$. The actual camber and ideal angle of attack of the sections was scaled by the desired section lift coefficient. The resulting 2D and 3D blade geometry is shown in figure 4.

3.1. Experimental results

Steady propeller performance tests were performed in the MIT water tunnel using the experimental setup shown in

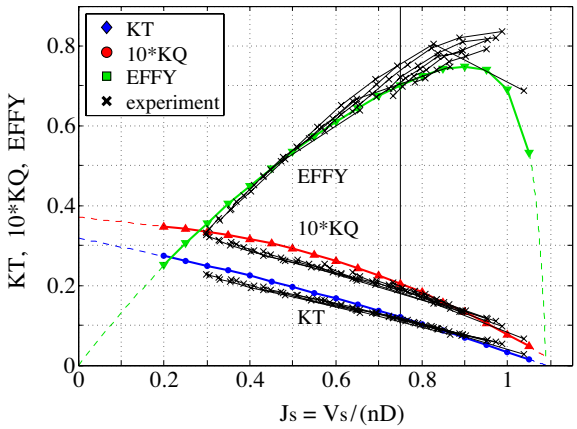

Figure 6. Off-design propeller performance curves, with experimental data. The design point is $J_s = 0.75$.

figure 5. The propeller was mounted on a trolling motor (Minn Kota motor assembly, part number 2069060) and situated in the water tunnel test section. Thrust and torque measurements were made for a range of steady flow speeds ($V_s = 0.1$ to 1.9 m/s) and steady rotation rates ($n = 1.4$ to 9.5 rev/s), spanning the advance ratios ($J_s = 0.3$ to 1.1). In these experiments, the flow speed was measured using the a laser Doppler velocimetry (LDV) system, and the drag on the motor housing, $F_{\text{motor drag}}(V_s)$, was inferred from the calibration data [Epps 2010]. The net force on the motor assembly was measured using the force dynamometer, so the thrust produced by the propeller was

$$T = k_f f_{\text{net force}} + F_{\text{motor drag}}(V_s) \tag{16}$$

where $k_f = 93.3$ [N/V] was the calibration.

The torque on the propeller was inferred from measurements of the current supplied to the motor, i_m, and of the angular velocity of the propeller

$$Q = k_m i_m - B(\omega) \tag{17}$$

where $k_m = 0.06454$ Nm/A, as determined by calibration tests. The steady rotation rate, ω, is the slope of a linear fit to the angular-position-versus-time data acquired from a Hall-effect sensor mounted to the motor assembly, and the friction torque, $B(\omega)$, was inferred from calibration data [Epps 2010]. These data are normalized in the usual way to form thrust and torque coefficients

$$K_T = \frac{T}{\rho n^2 D_p^4} \tag{18}$$

$$K_Q = \frac{Q}{\rho n^2 D_p^5} \tag{19}$$

where $D_p = 0.2487$m is the actual diameter of the printed propeller. The efficiency of the propeller is by definition

$$EFFY = \frac{TV_s}{Q\omega} = \frac{K_T J_s}{2\pi K_Q} \tag{20}$$

In figure 6, these data are plotted versus advance coefficient

$$J_s = \frac{V_s}{nD_p} \tag{21}$$

Figure 6 shows good agreement between the OPENPROP off-design performance predictions and the experimental results. The measured data match within 10% of the predicted performance for most advance ratios. These data provide valuable validation for the off-design performance analysis method.

3.2. Blade stresses

Since the performance predictions made by the off-design analysis model agree reasonably well with the measured performance data, these model predictions can be used to estimate the blade stresses. Blade normal stresses were estimated using the procedure outlined in Section 2.3. for the design state, as well as an off-design operating state, with $V_s = 1.5$ m/s, $n = 15$ rev/s, which corresponds to $J_s = 0.40$.

In figures 7 and 8, typical sign conventions for normal stress apply: tensile stresses are considered positive and compressive stresses negative. As expected, the off-design condition chosen shows higher stresses than the on-design condition. This is a result of (1) selecting an off-design design advance ratio where both KT and KQ are higher than on-design; and (2) achieving that off-design advance ratio with a higher rotation rate. (Had we chosen $J_s = 0.40$ with $V_s = 0.8$ m/s and $n = 8$ rev/s, then the stresses would be lower.)

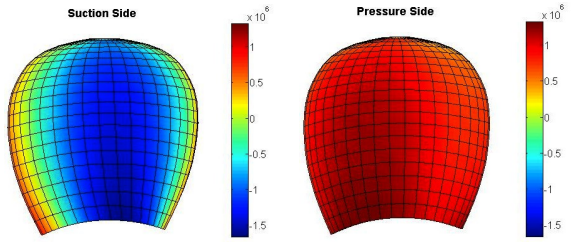

Figure 7. Blade stress for the on-design state: $J_s = 0.75$, $V_s = 1.5$ m/s, $n = 8$ rev/s, $D = 0.25$ m.

The stress estimates presented herein agree with the trends presented by Carlton [1994] for a symmetrical propeller blade without skew. Carlton [1994] presents isostress contour lines taken from FEA results, showing highest stress near the blade mid-chord in a region that extends close to the tip of the blade and a decreasing stress as one moves away from the mid-chord to the leading and trailing edges.

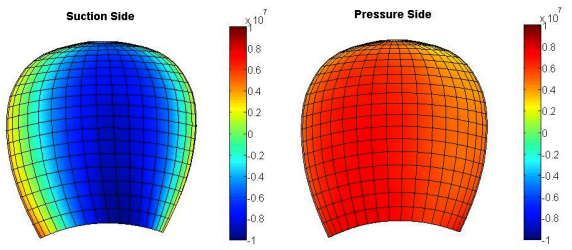

Figure 8. Blade stress for an off-design state: $J_s = 0.40$, $V_s = 1.5$ m/s, $n = 15$ rev/s, $D = 0.25$ m.

4. CURRENT RESEARCH FOCUS

Efforts are currently underway to extend the simple stress analysis presented herein to model large, flexible wind turbines. In the case of flexible blades, the vortex lattice will have to be augmented as to find the deflected state of the turbine, since blade flexure corresponds to a change in the geometry of the vortex lattice. This introduces 12 unknowns into the Newton solver, namely the (each 3-component) position, orientation, elemental forces, and elemental moments of each blade section. Also, for a large, flexible propeller or turbine, bending stresses due to rake and skew will have to properly be accounted for in the overall stress state of the blade.

One related study is of interest as well. The standard propeller lifting line model places the lifting line at the mid-chord and places the control points on the lifting itself. This offers computational efficiency, since the [Wrench 1957] formulae can be used to compute the induced velocities on the radial lifting line. One study of interest is to augment the vortex lattice such that the lifting line traces the quarter-chord of the blade sections and the control points are located at the three-quarter-chord positions, which is the standard model consistent with thin airfoil theory for flat-unswept wings. Comparison of performance predictions between the two vortex lattice geometries are of interest.

The OPENPROP project is intended to provide accurate and powerful propeller and axial flow turbine design codes for use by both novice users and experienced designers. The open-source nature of the code suite (published under the GNU public license protocol) is intended to make it a public resource to enhance the art of propeller and turbine design and analysis.

Acknowledgments This work is supported by the Office of Naval Research N000140810080 and NOAA NSG NA060AR4170019. In addition, the authors wish to thank Mr. Robert Damus of the Project Ocean, who was instrumental in securing funds that made some of this research possible.

REFERENCE

Abbott, I. H., and Von Doenhoff, A. E. *Theory of Wing Sections*. Dover, 1959.

Carlton, J. S. *Marine Propellers and Propulsion*. Butterworth-Heinemann, 1994.

Chung, H.-L. "An enhanced propeller design program based on propeller vortex lattice lifting line theory". M.S. thesis, MIT, 2007.

Coney, W.B. "A Method for the Design of a Class of Optimum Marine Propulsors". PhD thesis, MIT, 1989.

Drela, M. "XFOIL: An Analysis and Design System for Low Reynolds Number Airfoils." In: T.J. Mueller, editor. Low Reynolds Number Aerodynamics: Proceedings for the Conference, Notre Dame, Indiana, USA, 5-7 June 1989. Springer-Verlag, p. 1-12.

Epps, B.; Stanway, J.; and Kimball, R. "OPENPROP: An Open-Source Design Tool for Propellers and Turbines," SNAME Propeller and Shafting conference, 2009.

Epps, B.; Chalfant, J.; Kimball, R.; Techet, A.; Flood, K.; and Chryssostomidis, C., "OpenProp: An Open-source Parametric Design and Analysis Tool for Propellers," Proc. Grand Challenges in Modeling and Simulation (GCMS09), Istanbul, Turkey. July 13-16, 2009a.

Epps, B.P., "An Impulse Framework for Hydrodynamic Force Analysis: Fish Propulsion, Water Entry of Spheres, and Marine Propellers," Ph.D. Thesis, MIT, February 2010.

Kerwin, J.E. *Hydrofoils and Propellers*. MIT course 2.23 notes, 2007.

Kerwin, J.E. and Hadler, J.B., "Principles of Naval Architecture: Propulsion," SNAME, to appear 2010.

Ketcham, J. "Design, build and test of an axial flow, hydrokinetic turbine with fatigue analysis," Masters Thesis, MIT, May 2010.

Kimball, R.W. and Epps, B.P. OPENPROP v2.3 code, http://openprop.mit.edu, 2010.

Lerbs, H.W. "Moderately Loaded Propellers with a Finite Number of Blades and an Arbitrary Distribution of Circulation." Trans. SNAME, v. 60, 1952.

Peterson, C.J. "Minimum Pressure Envelope Cavitation Analysis Using Two-Dimensional Panel Method" M.S. Thesis, MIT, June 2008.

Wrench, J. W. "The calculation of propeller induction factors." Technical Report 1116, David Taylor Model Basin, February, 1957.